NASA CR-72843

TECHNICAL REPORT

AN INVESTIGATION OF STRAIN CYCLING BEHAVIOR OF 7075-T6 ALUMINUM UNDER COMBINED STATE OF STRAIN

THE EFFECTS OF OUT-OF-PHASE, BIAXIAL STRAIN CYCLING ON LOW CYCLE FATIGUE

by

S. Y. Zamrik

Department of Engineering Mechanics
The Pennsylvania State University
University Park, Pennsylvania

National Aeronautical Space Administration
Research Grant NGR-39-009-034

January 5, 1972

NASA CR-72843

Technical Report

An Investigation of Strain Cycling Behavior of 7075-T6 Aluminum Under Combined State of Strain

The Effects of Out-of-Phase, Biaxial Strain Cycling on Low Cycle Fatigue

by

S. Y. Zamrik

Department of Engineering Mechanics
The Pennsylvania State University
University Park, Pennsylvania

National Aeronautical Space Administration
Research Grant NGR-39-009-034

January 5, 1972

Preface

This technical report covers the research program on the effect of out-of-phase strain cycling on the low cycle fatigue of biaxially loaded specimens. A method to apply phase angles between two strains imposed in two different directions was developed at the fatigue laboratory of the Engineering Mechanics of the Pennsylvania State University. The reported test data and the proposed theoretical analysis are part of a research program on "biaxial strain cycling effect on fatigue life of structural materials" supported by the National Aeronautics and Space Administration, Lewis Research Center, under grant NGR-39-009-034.

Table of Contents

List of Illustrations

Nomenclature

N	Cycles to failure
σ	Stress
ε	Strain
ε_T	Total strain
E	Modulus of elasticity in tension
ε_f	Strain at fracture
ε_{el}	Elastic strain
$\varepsilon_1, \varepsilon_2, \varepsilon_3$	Principal strains
μ	Poisson's ratio
γ_{oct}	Octahedral shear strain
ε_x	Applied axial strain in the x direction
γ_{xy}	Applied torsional strain
ϕ	Phase angle between applied strains
ω	Frequency of straining
t	Time
ε_y	Strain in the y direction
ε_z	Strain in the z direction
ε''_x	Maximum applied axial strain
γ''_{xy}	Maximum applied torsional strain
ε''_T	Maximum total strain
$\varepsilon''_1, \varepsilon''_2, \varepsilon''_3$	Principal strains necessary to produce ε''_T
ε'_x	Applied axial strain necessary to produce ε''_T
γ'_{xy}	Applied torsional strain necessary to produce ε''_T

Abstract

The effects of out-of-phase or non-synchronous straining on low cycle fatigue was investigated. Biaxial strains were imposed on thin-walled tubular 7075-T6 aluminum specimens by tension - compression and torsion. Phase angles of 0°, 30°, 45°, 60°, and 90° were applied between two strains. It was found that out-of-phase cycling has an effect on the failure mode in the low cycle fatigue range. An analysis based on the maximum total strain in three dimensional strain is proposed for treating "out-of-phase" straining conditions in low cycle fatigue.

The Effects of Out-of-Phase, Biaxial Strain Cycling on Low Cycle Fatigue

1. Introduction

In certain engineering applications, structural elements encounter non-synchronous loading systems that result in out-of-phase straining conditions. Aircraft structure, for example, are vulnerable to such straining conditions, in which case reduction of fatigue life may be encountered. Most of the fatigue data in uniaxial or biaxial loading systems do not treat this subject because of the experimental difficulty in loading a specimen simultaneously with two independent non-synchronous strains in two directions. The only significant study related to this investigation was a publication by Taira, et al(1), in 1968. They investigated the low cycle fatigue failure of tubular specimens subjected to combined cyclic torsion and out-of-phase cyclic tension - compression at a temperature of 450°C; however their investigation was limited to 90° phase angle. A modified "equivalent strain range" concept, was proposed for "out-of-phase" strain conditions.

The experimental investigation presented in this report deals with a number of phase angles ranging from 0° to 90°. A theoretical analysis, based on a strain tensor for a biaxial loading condition of a thin-walled tube, is proposed for out-of-phase cyclic strain condition. The experimental results show a particular phase effect on crack growth and failure mode in the selected low cycle fatigue

range.

2. Material Tested and Specimens

The material used in the investigation was 7075-T6 aluminum alloy extruded in tubular form with an inside diameter of one inch and a nominal wall thickness of one-quarter inch. The specimen was machined down to a wall thickness of 0.050 inch over a gauge length of 1.10 inches and the transition fillets had a radius of 0.05 inches. Figure 1 shows a typical tubular specimen with pertinent dimensions. The mechanical properties of the material tested are presented in Table 1.

3. Test Equipment

The electro-hydraulic closed loop testing machine used in this study is totally unique in its capabilities. The machine was designed specifically to test thin-walled tubes under various fatigue loading conditions. Since the axial loading system is completely independent from the torsional system, various ratios between axial and torsional strains can be imposed in- or out-of-phase. The out-of-phase strains capability ranges from 0 to 180°. A schematic diagram, shown in Figure 2, shows the basic units of the equipment and the relation between the components. Figure 3 shows the testing equipment.

The most significant component in the schematic diagram is the template of two Linear Variable Differential Transformers that

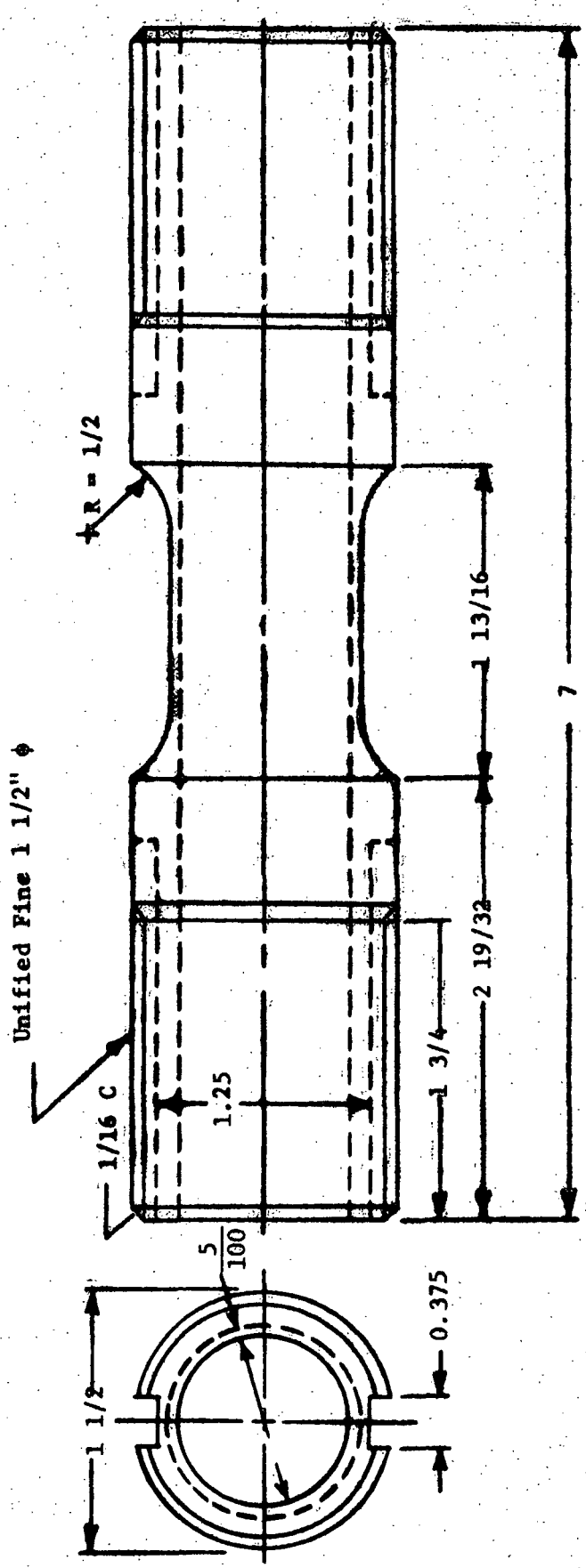

Figure 1. Fatigue Specimen.

Table 1. Chemical Composition and Mechanical Properties of 7075-T6 Aluminum.

Chemical Composition	Percent
Cu	1.2
Mg	2.1
Mn	0.3
Fe	0.7
Si	0.5
Zn	5.1
Cr	0.2
Ti	0.2
Al	Remainder
Mechanical Properties	
Yield Stress (0.2% strain)	69 Ksi
Ultimate Stress	79 Ksi
Ductility (2 inches gage)	11 %
Modulus of Elasticity	$10.3X10^3$ Ksi
Poisson's Ratio	.321

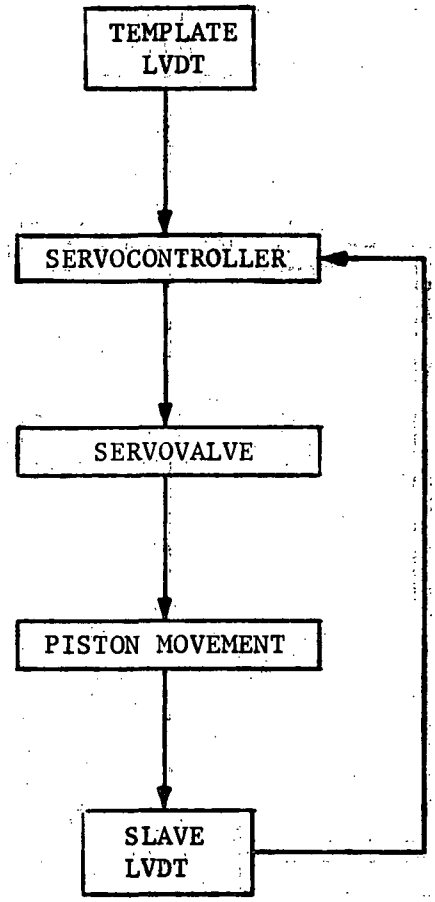

Figure 2. Block Diagram of Biaxial Fatigue Testing Machine.

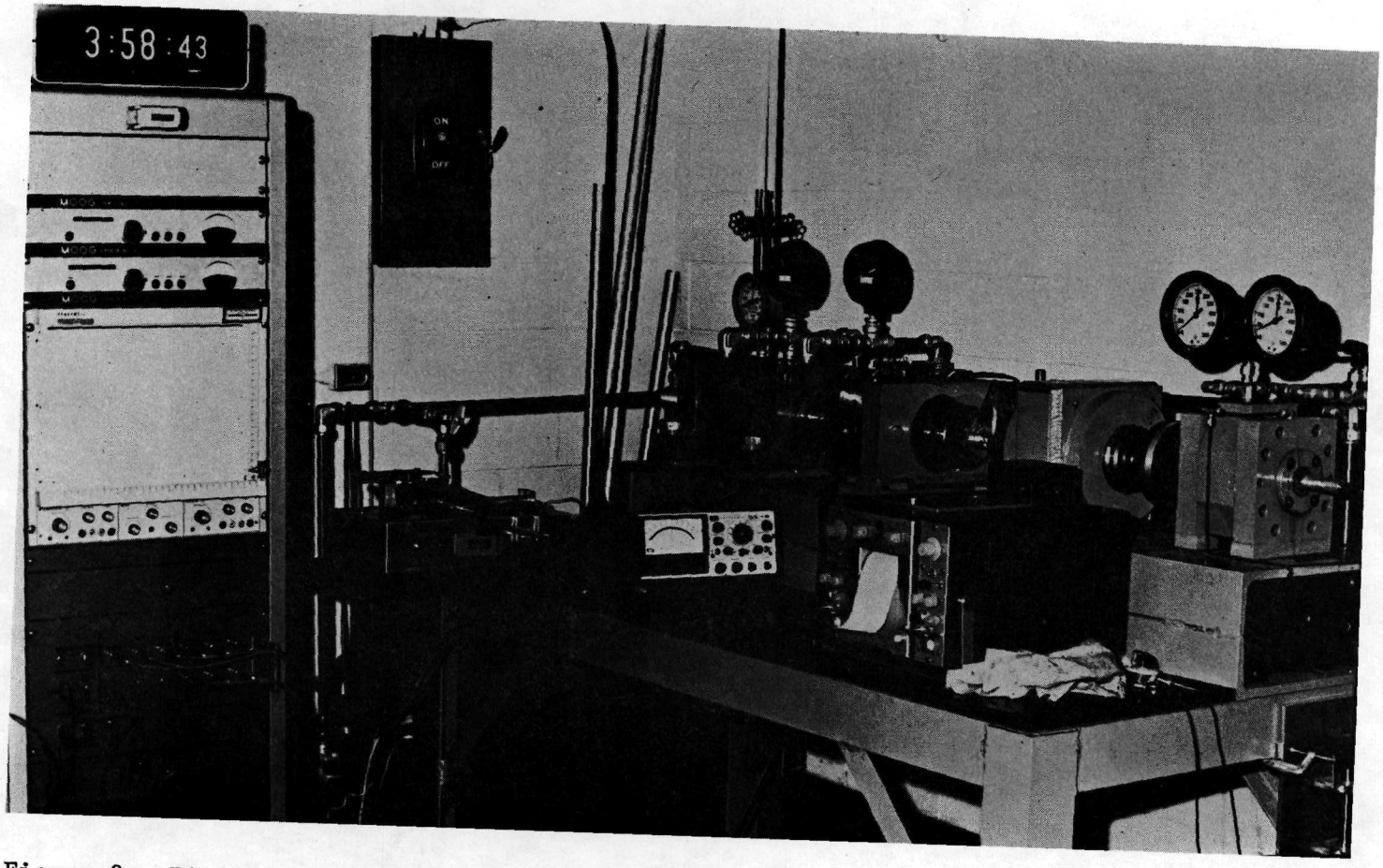

Figure 3. Biaxial Strain Cycling Fatigue Machine.

are connected in parallel. This network enables the adjustment of the zero position of the LVDT electronically rather than by physically moving the transformer. The core of one LVDT is connected to a micrometer which facilitates the adjustment of the system. The other LVDT core is connected to a cam which is rotated by an electric motor at a speed of 7-3/4 revolutions per minute. Thus the axial and torsional template LVDT's networks are driven by the same cam and electric motor; Therefore, the phase angle between the template output signals and consequently, the strains applied to the specimen can be adjusted by rotating one LVDT in circular motion around the motor. Figure 4 shows the template unit where one LVDT, mounted on a protractor, was rotated to 90° with respect to the other. The cores of the visible LVDT's are connected to a cam and motor system located directly beneath the center of the protractor. The protractor enables the "dialing" of any desired phase angle into the system.

Also mounted on the template chassis is a microswitch which is tripped everytime the cam makes one revolution. The signal from the microswitch is used to operate the cycle counter for the system.

The output signal from this system determines the motion of the machine. By changing the motor speed, the speed of loading is changed; by changing the angle of the protractor, the phase angle is changed; by changing the zero position with the micrometers, the mean strain condition is altered. It should be noted that because the system is operated by a cam, the imposed loads are sinusoidal. However, any desired wave form can be imposed on the specimen by merely

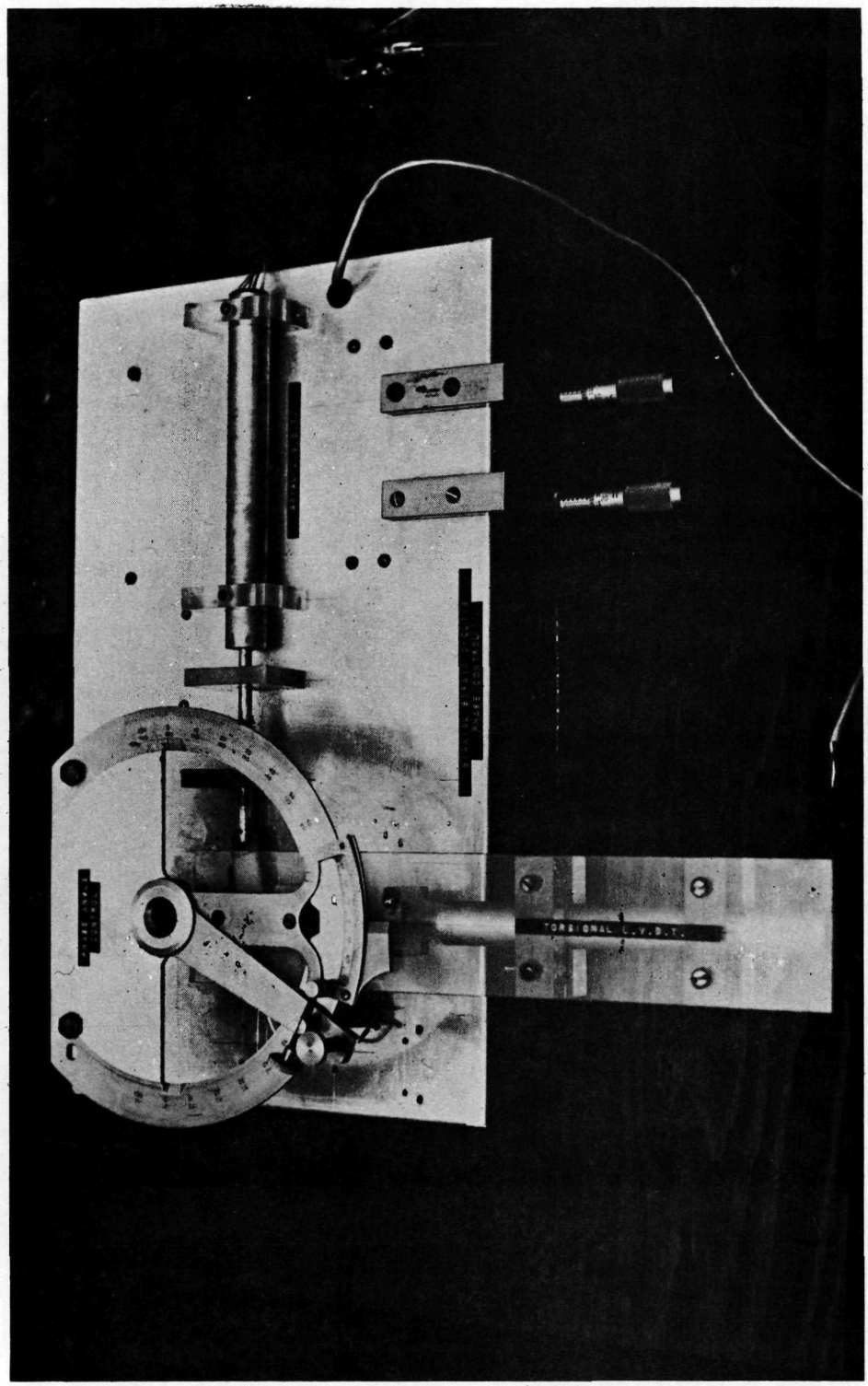

Figure 4. Biaxial Strain Cycling Phase Controller

changing this cam motor arrangement.

The output signal from the template system is fed into servo-control units mounted in the relay rack in Figure 3. In this unit, the signal from the template is compared with the signal from the feedback or slave LVDT. The ratio of the amplitudes between the template signal and the feedback LVDT can be adjusted with the ratio potentiometer in the servocontrol circuit. Thus, while the template signal can have constant amplitude, the servocontrol unit can adjust this signal to produce larger or smaller strains in the machine. Furthermore, by setting the axial ratio potentiometer at a different setting than the ratio potentiometer in the torsional servocontroller circuit, any ratio between maximum axial and maximum torsional strain can be imposed.

The difference of the compared signals is fed from the servo-controller unit into the servovalves; causing the servovalve to switch the hydraulic pressure from one side of the piston to the other. This action causes the specimen to be strained according to the signal applied to the servovalve.

Mounted on the axial piston of the fatigue machine were a series of strain gages. These gages were used as a load monitoring system and were only used to setup the specimen. The torsional and axial testings were strain controlled.

4. Maximum Total Strain for Out-of-Phase Strains

A surface element of a thin-walled tube under a combined

loading system, as shown in Figure 5, will encounter a strain distribution that can be expressed by a strain tensor in the form of:

$$\begin{vmatrix} \varepsilon_x & \frac{\gamma_{xy}}{2} & 0 \\ \frac{\gamma_{xy}}{2} & \varepsilon_y & 0 \\ 0 & 0 & \varepsilon_z \end{vmatrix} \tag{1}$$

where ε_x, ε_y, ε_z and γ_{xy} are engineering strains. Since the thin-walled tube is under axial and torsional strains, the strain in the y-direction and z-direction are:

$$\begin{aligned} \varepsilon_y &= -\mu\varepsilon_x \\ \varepsilon_z &= -\mu\varepsilon_x \end{aligned} \tag{2}$$

where μ is Poisson's ratio.

In low-cycle fatigue, the applied strains are well into the plastic region of a material stress-strain curve, therefore the constant volume assumption can be used where $\mu = 1/2$, or:

$$\varepsilon_x + \varepsilon_y + \varepsilon_z = 0 \tag{3}$$

The diagonalization of the strain tensor, Equation (1),

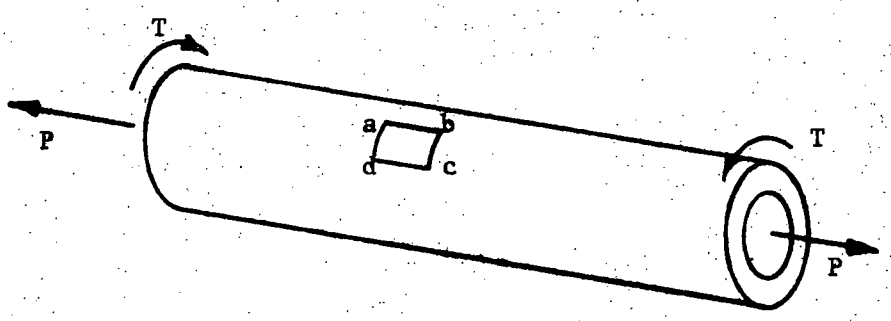

(a) Combined Loading System - Tubular Specimen

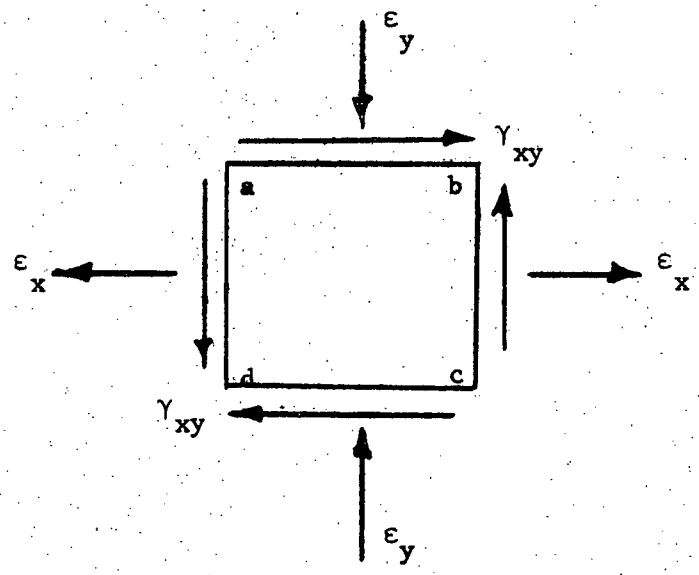

(b) Surface Element Showing Strain under Combined Loading System

Figure 5. Tubular Specimen and Surface Element - Biaxial Loading System.

yields the three principal strain equations:

$$\varepsilon_1 = \frac{1}{2}[(\varepsilon_x - \mu\varepsilon_x) + \sqrt{(\varepsilon_x + \mu\varepsilon_x)^2 + \gamma_{xy}^2}]$$

$$\varepsilon_2 = \frac{1}{2}[(\varepsilon_x - \mu\varepsilon_x) - \sqrt{(\varepsilon_x + \mu\varepsilon_x)^2 + \gamma_{xy}^2}] \qquad (4)$$

$$\varepsilon_3 = -\mu\varepsilon_x$$

The exactness of Equations(4) can be checked by taking Poisson's ratio equals to one half. Therefore the sum of the diagonal terms of any of the strain tensor should add up to zero, then:

$$\varepsilon_1 + \varepsilon_2 + \varepsilon_3 = 0 \qquad (5)$$

or

$$\frac{1}{2}[(\varepsilon_x - \frac{1}{2}\varepsilon_x) + \sqrt{(\varepsilon_x + \frac{1}{2}\varepsilon_x)^2 + \gamma_{xy}^2}]$$

$$+ \frac{1}{2}[(\varepsilon_x - \frac{1}{2}\varepsilon_x) - \sqrt{(\varepsilon_x + \frac{1}{2}\varepsilon_x)^2 + \gamma_{xy}^2}] - \frac{1}{2}\varepsilon_x = 0 \qquad (6)$$

Equation (6) yields:

$$\frac{1}{4}\varepsilon_x + \frac{1}{4}\varepsilon_x - \frac{1}{2}\varepsilon_x = 0 \qquad (7)$$

Thus the exactness of Equations (4) is met.

Most of the analyses presented in low cycle fatigue studies, have utilized some type of range calculation in interpreting the

experimental data. However, when biaxial out-of-phase straining is encountered, a consequent rotation of principal axes occurs, and the orientation of the element for which the principal strains occur will vary with time. Therefore the question arises as to how one can calculate a range value. If maximum and minimum values of strain occur at different times, then they also occur in different directions; therefore, for any type of range calculation, the maximum and minimum strain must be projected onto a common direction, resulting in a great difficulty in determining the exact values of maximum and minimum strains. However if one considers only the maximum total strain value, the question of range values, direction of strains can be eliminated. In this case, the total strain ε_T for three dimensional strain field is defined as:

$$\varepsilon_T = \sqrt{\varepsilon_1^2 + \varepsilon_2^2 + \varepsilon_3^2} \tag{8}$$

For a sinusoidal in-phase straining condition; the imposed strains, shown in Figure 6, are:

$$\varepsilon_x = \varepsilon_x'' \sin \omega t$$

$$\gamma_{xy} = \gamma_{xy}'' \sin \omega t \tag{9}$$

and for out-of-phase straining conditions as shown in Figure 7:

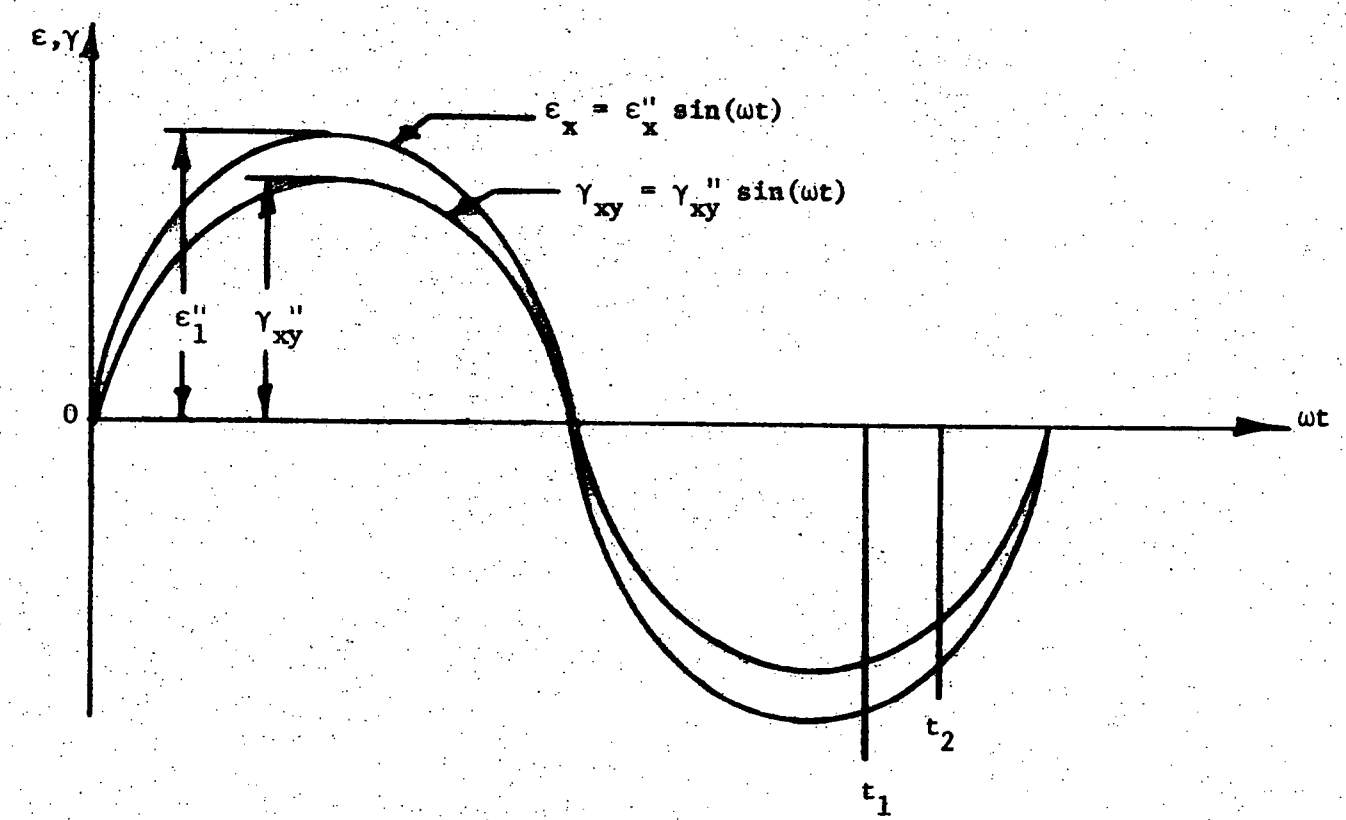

Figure 6. Strain versus Time for In-Phase Relation of ε_x and γ_{xy}.

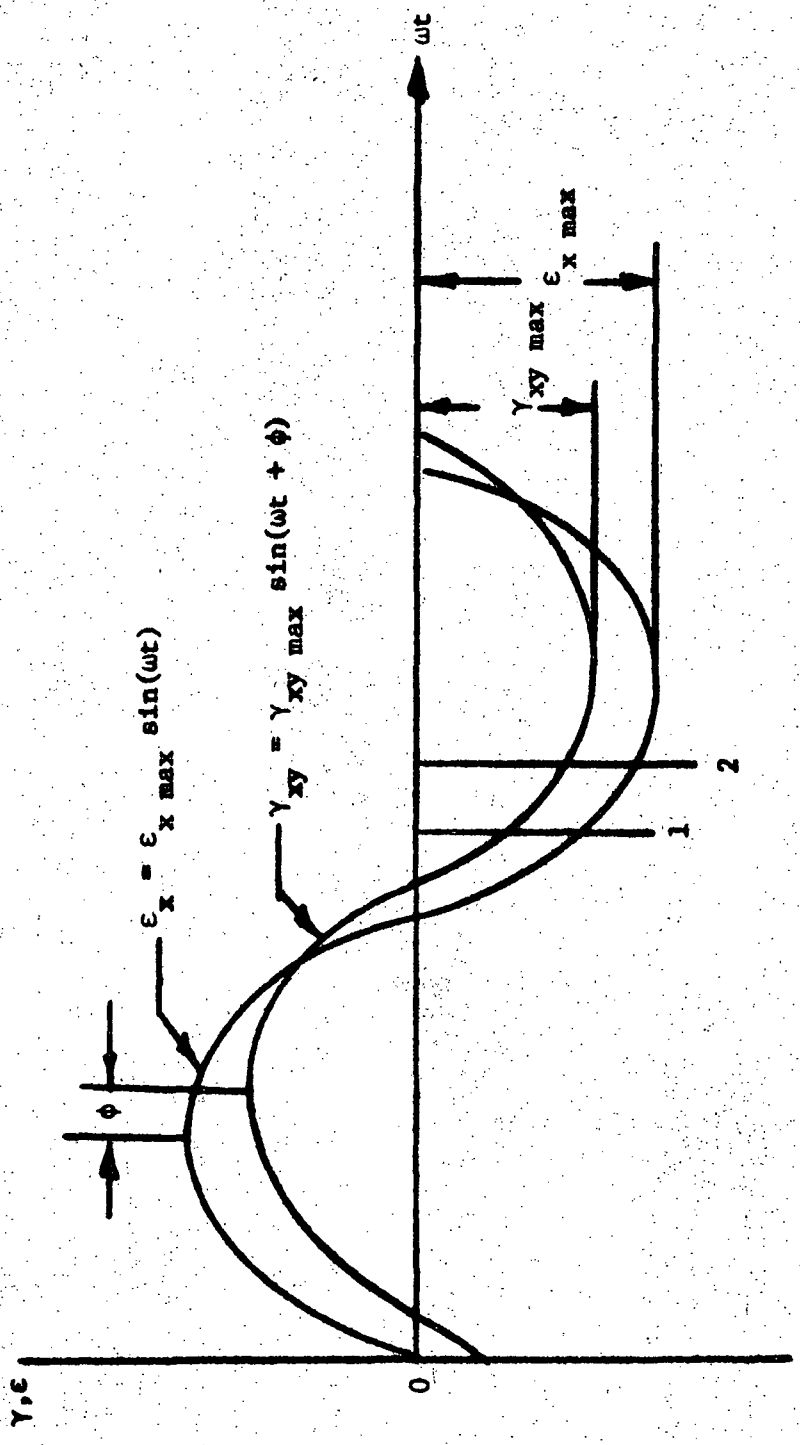

Figure 7. Strain versus Time for Out-of-Phase Straining Condition.

$$\varepsilon_x = \varepsilon''_x \sin \omega t$$

$$\gamma_{xy} = \gamma''_{xy} \sin(\omega t + \phi) \tag{10}$$

where ϕ is the phase angle.

Substituting Equations (10) into (4) and then the resulting equation into (8), the total strain becomes:

$$\varepsilon_T = \{[\tfrac{1}{2}([\varepsilon''_x \sin \omega t - \mu\varepsilon''_x \sin \omega t] + \sqrt{(\varepsilon''_x \sin \omega t + \mu\varepsilon''_x \sin \omega t)^2 + (\gamma''_{xy} \sin(\omega t + \phi))^2})]^2 + [\tfrac{1}{2}([\varepsilon''_x \sin \omega t - \mu\varepsilon''_x \sin \omega t] - \sqrt{(\varepsilon''_x \sin \omega t + \mu\varepsilon''_x \sin \omega t)^2 + (\gamma''_{xy} \sin(\omega t + \phi))^2})]^2 + [-\mu\varepsilon''_x \sin \omega t]^2\}^{1/2} \tag{11}$$

Equation (11) was maximized through the use of the digital computer for different times t. In the computer program, the values of ε_T were calculated starting at t = 0.1 seconds and adding 0.1 seconds for each new calculation of ε_T for a total of 78 iterations. Since the frequency of straining was 7.75 revolutions per minute, or one cycle of straining every 7.75 seconds the 78 iterations of time used in calculating ε_T covered one complete cycle of straining.

From this program, the maximum value of ε_T, designated as ε_T'', was recorded with the time when it occured and with the values of ε_1, ε_2 and ε_3 which produced ε_T''.

5. Experimental Results and Observations

The experimental testing program conducted for this investigation was carried out in two parts. First part involved uniaxial tests and pure torsional tests. The results of the two separate tests were used as control data for the combined loading condition. The second series of tests consisted of biaxial loading at phase angles of 0°, 30°, 45°, 60°, and 90°.

The results of both series of tests are presented in Appendix A. The test results include the measured values of the maximum axial and torsional deformation, the calculated strains, the calculated maximum total strain, and the number of cycles to failure. With the experimental values, the maximum total strain ε_T'' was found by utilizing the computer program based on Equations (10) and (11).

Figure 8 shows the maximum total strain ε_T'' versus the number of cycles to failure. The solid line drawn through the data points is the interpolated result of all tests and the dashed line indicates the extrapolation of test data into the region less than five cycles. The data points are plotted according to phase angle as indicated by the various symbols around the plotted points.

In order to check the extrapolated result of the data, the value of the maximum total strain for a static tension was invest-

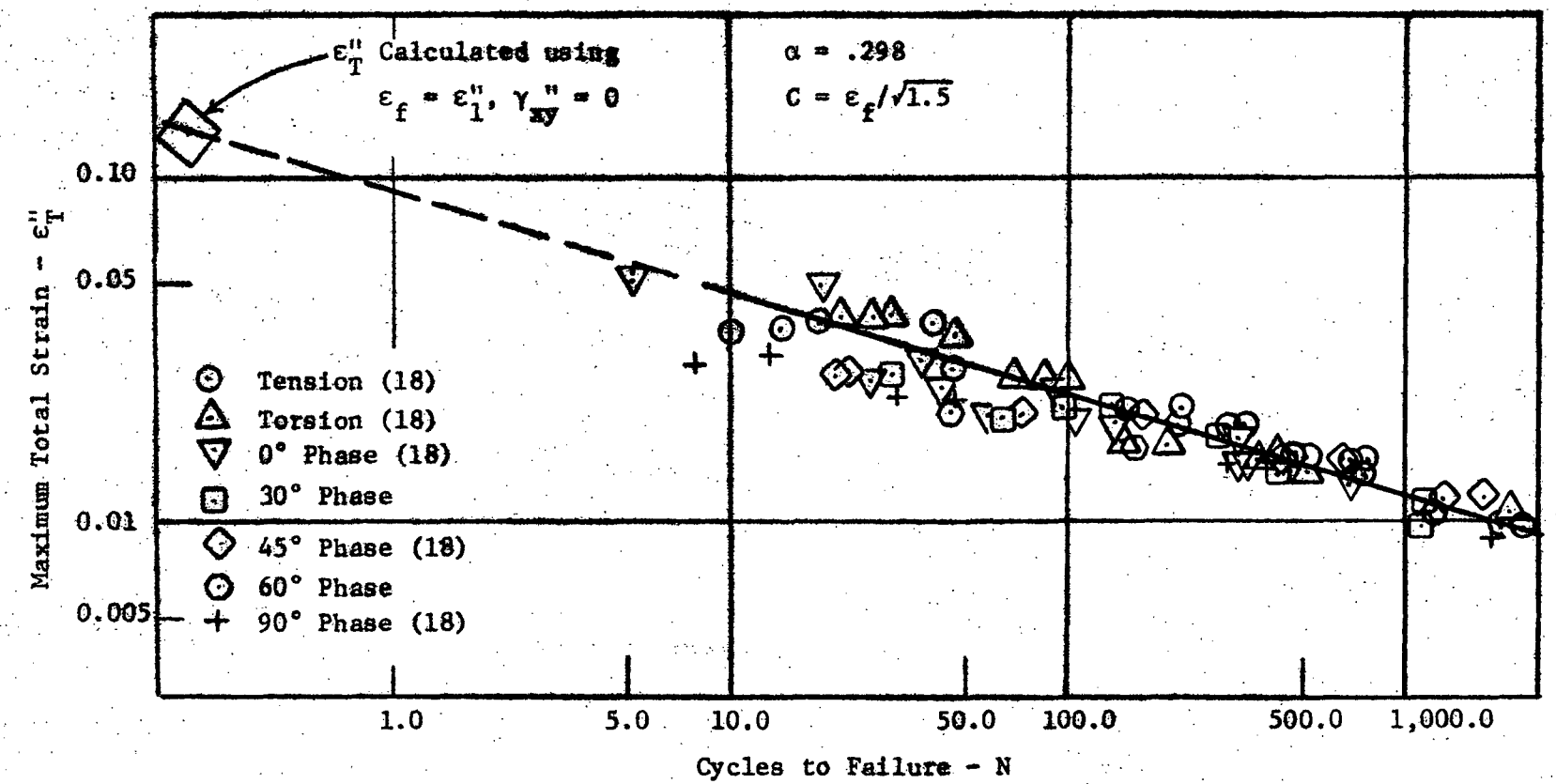

Figure 8. Maximum Total Strain versus Cycles to Failure using Experimental Data from Various Phase Angle Tests. Both Coordinates are Logarithmic.

igated. For a static tension test, the value of cycles to failure is 1/4, and the value of ε_x, the applied axial strain, is equal to the fracture ductility. In this case it is 0.11 inches per inch as obtained from Table 1, with a shear strain, γ_{xy} of zero. Using these values, the maximum total strain is equal to 0.135 inches per inch. This value represents the static tension total maximum strain ε_T'' and it is indicated by the large triangle at the one-quarter cycle point on Figure 8. It falls exactly on the extrapolated line of the experimental data.

The scattering of data on Figure 8 is of interest. The data in the region less than 60 cycles to failure is considerably more scattered than the data between 60 and 10^3 cycles. This deviation is due to the fact that in tubular specimens under high strains, the tube walls will buckle. Therefore, the scatter of data for cyclic lives less than 60 cycles is believed to be due to buckling of the specimen walls, and examination of the specimens tested in this region showed signs of buckling.

The interpolated line in Figure 8 follows a power law relationship that can be expressed in the form of:

$$\varepsilon_T'' N^{\alpha} = C \qquad (12)$$

where C is the intercept of the interpolated line at N = 1, and α is the slope of the line. The value of C in this investigation was found to be $1/\sqrt{1.5}$ times the fracture ductility ε_f. This agrees

closely with Manson's concept of plastic strain range and its relation to number of cycles to failure(2). The value of the slope of the strain-cycles diagram on logarithmic coordinates was found to be approximately 0.3. This value varies considerably from the value of 1/2 for uniaxial strain range slopes, however it is consistent with the octahedral shear strain range concept as proposed by the author(3). In this case for Poisson's ratio equals to 1/2, the total strain as indicated by Equation (10) is equivalent to the octahedral shear strain.

The interpolated line of Figure 8 may also be determined from a series of low-cycle uniaxial tests. These tests are indicated by circles. The interpolated line follows these points fairly closely while data points for biaxial loading fall close to the interpolated line in the region between 60 and 1,000 cycles. Hence, for any given material, the behavior of the material under biaxial loading conditions can be predicted from a series of uniaxial tests if the maximum total strain equation as proposed in this report is utilized. This is also true in the case of the octahedral shear strain range concept. One can state that a material will experience fatigue failure in N cycles under biaxial, out-of-phase loading conditions if maximum total strain as expressed in Equation (10) equals the value necessary to produce fatigue failure in N cycles in a uniaxial test.

Examination of failed specimens under out-of-phase biaxial strain conditions revealed that the crack leading to failure took different orientation. This effect can be seen in Figure 9 where a

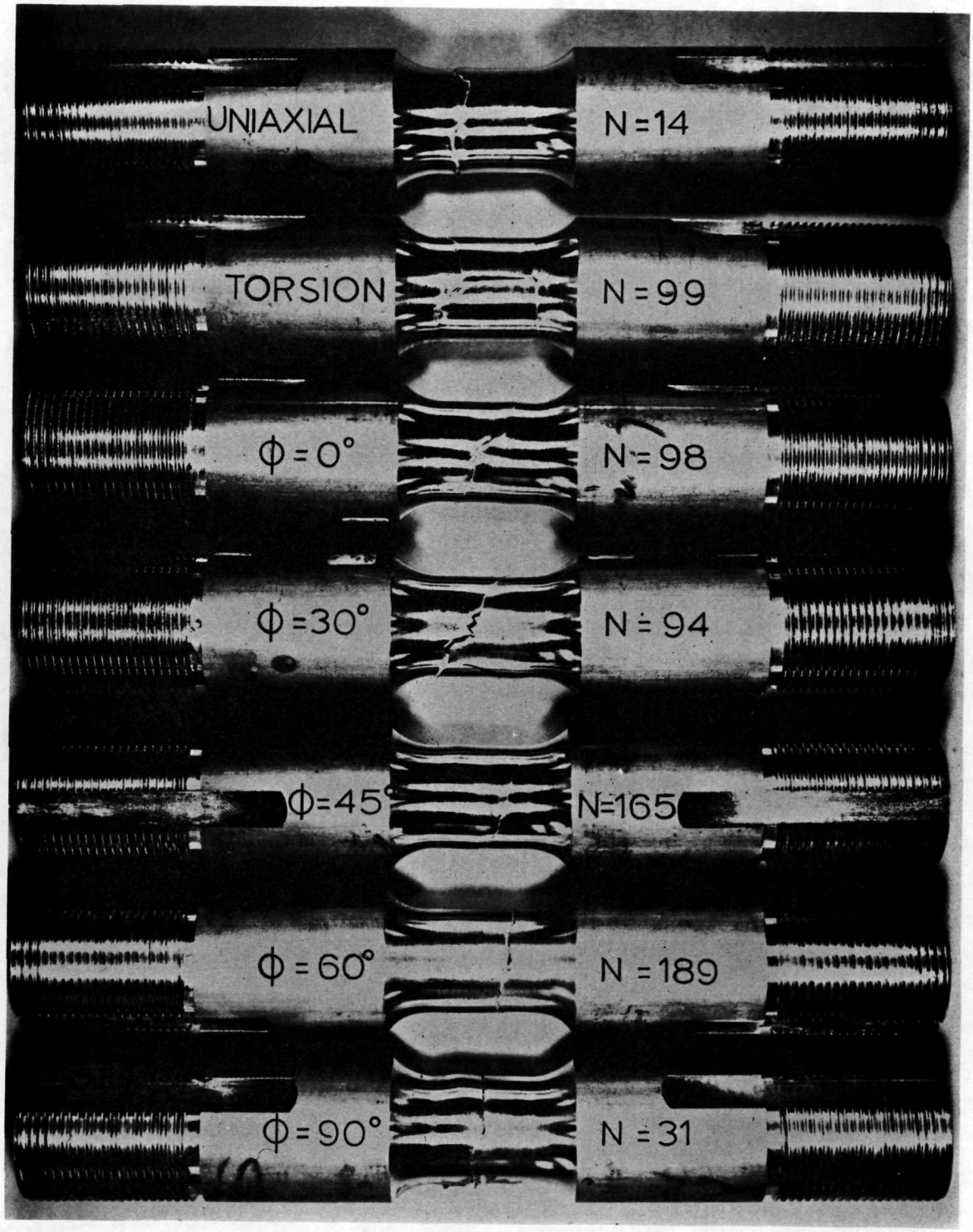

Figure 9. Variation of Crack Angle for Different Phase Angles.

comparison of uniaxial, torsional and the combination of these two loadings under a variety of phase angles shows the orientation of the crack to achieve a 45° inclination for phase angle of 30° and then reverses itself to 90° orientation for a phase angle of 90°. The failure mode under 90° phase angle was similar to the failure mode under uniaxial straining condition. This observation could lead to an error in assuming that phase angles have no effect on low cycle fatigue. Tests conducted under 0°, 30°, 45°, and 60° shows clearly this assumption is not true and that a definite phase effect on the failure mode exists.

6. Conclusions

The research program sponsored under NASA Grant NGR 39-009-034 dealt with the effect of out-of-phase biaxial strain cycling. It was found that a power law relationship based on the maximum total strain in a three dimensional strain field can be expressed as:

$$\varepsilon_T'' \, N^{\alpha} = C$$

The maximum total strain ε_T'' was derived from applied strains through the use of Equation (11) which is also equivalent to the octahedral shear strain theory when the value of Poisson's ratio equals to 1/2. Test data and specimen mode of failure shows definite phase angle effect on biaxial low cycle fatigue and if the phase angle was not accounted for, a considerable error may result in the analysis that

may be used for in-phase cycling condition. It was also found that uniaxial low cycle fatigue can be correlated to biaxial strain cycling.

The out-of-phase biaxial strain cycling produces a rotation of the principal strain axes and the surface element takes a new orientation where maximum and minimum strains occur at different times.

It should be pointed out that the proposed analysis and the experimental data does not account for any mean strain effect.

7. Acknowledgements

The investigator gratefully acknowledges the assistance of Messrs. O. G. Mizuhata and R. Frishmuth in conducting the tests. These tests were part of their thesis programs conducted under the supervision of the author.

References

1. Taira, S., Inoue, T. and Yoshida, T., "Low-cycle Fatigue under Multiaxial Stresses", 11th Congress JSME, pp. 60-65, March 1968.

2. Manson, S. S., Thermal Stress and Low Cycle Fatigue, McGraw-Hill Book Co., Inc., New York, 1966.

3. Zamrik, S. Y., and Goto, T., "The Use of Octahedral Shear Strain Theory in Biaxial Low Cycle Fatigue", in Proceedings of the First Inter-American Conference on Materials Technology, ASME, pp. 551-562, New York, 1968.

Appendix A

Experiment Results

APPENDIX A

EXPERIMENTAL DATA AND CALCULATED VALUES

Measured Maximum Axial Deformation	Measured Maximum Torsional Deformation	Calculated Maximum Axial Strain	Calculated Maximum Torsional Strain	Calculated Maximum Total Strain	Measured Cycles to Failure
Phase Angle - 0° Pure Tension					
0.0319	0.0	0.0290	0.0000	0.0355	10
0.0324	0.0	0.0295	0.0000	0.0361	14
0.0341	0.0	0.0310	0.0000	0.0379	18
0.0248	0.0	0.0225	0.0000	0.0275	39
0.0242	0.0	0.0220	0.0000	0.0269	45
0.0187	0.0	0.0170	0.0000	0.0208	142
0.0160	0.0	0.0150	0.0000	0.0184	212
0.0187	0.0	0.0170	0.0000	0.0208	218
0.0160	0.0	0.0150	0.0000	0.0184	298
0.0160	0.0	0.0150	0.0000	0.0183	316
0.0138	0.0	0.0125	0.0000	0.0153	460

APPENDIX A (cont'd)

Measured Maximum Axial Deformation	Measured Maximum Torsional Deformation	Calculated Maximum Axial Strain	Calculated Maximum Torsional Strain	Calculated Maximum Total Strain	Measured Cycles to Failure
0.0138	0.0	0.0125	0.0000	0.0153	468
0.0138	0.0	0.0125	0.0000	0.0153	487
0.0132	0.0	0.0120	0.0000	0.0147	679
0.0126	0.0	0.0115	0.0000	0.0141	727
0.0121	0.0	0.0110	0.0000	0.0135	739
0.0123	0.0	0.0112	0.0000	0.0137	759
0.0093	0.0	0.0085	0.0000	0.0104	1196
0.0090	0.0	0.0082	0.0000	0.0100	1913
0.0082	0.0	0.0075	0.0000	0.0092	2169
Phase Angle - 0° Pure Torsion					
0.0	0.0810	0.0000	0.0540	0.0405	21
0.0	0.0810	0.0000	0.0540	0.0405	27
0.0	0.0825	0.0000	0.0550	0.0412	29

APPENDIX A (cont'd)

Measured Maximum Axial Deformation	Measured Maximum Torsional Deformation	Calculated Maximum Axial Strain	Calculated Maximum Torsional Strain	Calculated Maximum Total Strain	Measured Cycles to Failure
0.0	0.0706	0.0000	0.0472	0.0354	45
0.0	0.0545	0.0000	0.0357	0.0268	68
0.0	0.0522	0.0000	0.0348	0.0261	84
0.0	0.0433	0.0000	0.0289	0.0217	96
0.0	0.0545	0.0000	0.0357	0.0268	99
0.0	0.0358	0.0000	0.0238	0.0178	143
0.0	0.0358	0.0000	0.0238	0.0178	198
0.0	0.0315	0.0000	0.0210	0.0157	357
0.0	0.0315	0.0000	0.0210	0.0157	375
0.0	0.0280	0.0000	0.0187	0.0140	517
0.0	0.0280	0.0000	0.0187	0.0140	610
0.0	0.0230	0.0000	0.0153	0.0115	2000

APPENDIX A (cont'd)

Measured Maximum Axial Deformation	Measured Maximum Torsional Deformation	Calculated Maximum Axial Strain	Calculated Maximum Torsional Strain	Calculated Maximum Total Strain	Measured Cycles to Failure
Phase Angle - 0°					
0.0286	0.0391	0.0260	0.0261	0.1992	4
0.0253	0.0570	0.0230	0.0380	0.0404	5
0.0273	0.0570	0.0248	0.0380	0.0419	5
0.0127	0.0987	0.0115	0.0657	0.0516	18
0.0165	0.0384	0.0150	0.0256	0.0268	26
0.0236	0.0261	0.0215	0.0174	0.0295	37
0.0154	0.0350	0.0140	0.0233	0.0246	42
0.0099	0.0356	0.0090	0.0238	0.0212	58
0.0198	0.0219	0.0180	0.0146	0.0247	90
0.0110	0.0338	0.0100	0.0225	0.0210	98
0.0099	0.0338	0.0090	0.0225	0.0203	138
0.0143	0.0163	0.0130	0.0109	0.0180	308

APPENDIX A (cont'd)

Measured Maximum Axial Deformation	Measured Maximum Torsional Deformation	Calculated Maximum Axial Strain	Calculated Maximum Torsional Strain	Calculated Maximum Total Strain	Measured Cycles to Failure
0.0049	0.0280	0.0045	0.0187	0.0152	311
0.0088	0.0223	0.0080	0.0149	0.0150	330
0.0076	0.0192	0.0069	0.0128	0.0129	661
0.0066	0.0171	0.0060	0.0114	0.0114	1144
Phase Angle - 30°					
0.0190	0.0350	0.0173	0.0234	0.0268	30
0.0150	0.0260	0.0136	0.0173	0.0206	61
0.0050	0.0445	0.0045	0.0296	0.0228	94
0.0045	0.0425	0.0041	0.0283	0.0218	137
0.0115	0.0270	0.0104	0.0180	0.0181	274
0.0092	0.0227	0.0084	0.0151	0.0149	411
0.0025	0.0187	0.0023	0.0125	0.0098	775
0.0060	0.0150	0.0055	0.0099	0.0098	1073

APPENDIX A (cont'd)

Measured Maximum Axial Deformation	Measured Maximum Torsional Deformation	Calculated Maximum Axial Strain	Calculated Maximum Torsional Strain	Calculated Maximum Total Strain	Measured Cycles to Failure
Phase Angle - 45°					
0.0193	0.0397	0.0175	0.0265	0.0272	20
0.0198	0.0412	0.0180	0.0275	0.0281	21
0.0154	0.0292	0.0140	0.0195	0.0210	72
0.0162	0.0261	0.0147	0.0174	0.0208	165
0.0105	0.0219	0.0095	0.0146	0.0147	404
0.0107	0.0219	0.0097	0.0146	0.0150	636
0.0079	0.0184	0.0072	0.0123	0.0119	1229
0.0086	0.0178	0.0078	0.0119	0.0122	1660
Phase Angle - 60°					
0.0165	0.0335	0.0150	0.0223	0.0217	44
0.0090	0.0265	0.0082	0.0177	0.0148	125
0.0130	0.0250	0.0118	0.0167	0.0167	148

APPENDIX A (cont'd)

Measured Maximum Axial Deformation	Measured Maximum Torsional Deformation	Calculated Maximum Axial Strain	Calculated Maximum Torsional Strain	Calculated Maximum Total Strain	Measured Cycles to Failure
0.0076	0.0225	0.0069	0.0150	0.0125	189
0.0115	0.0250	0.0104	0.0167	0.0156	502
0.0062	0.0190	0.0056	0.0126	0.0104	1009
Phase Angle - 90°					
0.0253	0.0480	0.0230	0.0320	0.0282	8
0.0275	0.0418	0.0250	0.0279	0.0306	13
0.0203	0.0375	0.0185	0.0250	0.0226	31
0.0204	0.0344	0.0186	0.0229	0.0228	45
0.0126	0.0248	0.0115	0.0165	0.0141	294
0.0121	0.0254	0.0110	0.0169	0.0135	366
0.0071	0.0240	0.0065	0.0140	0.0105	436
0.0086	0.0164	0.0078	0.0109	0.0096	1034
0.0077	0.0156	0.0070	0.0105	0.0086	1747

External Distribution

1. Library (2)
   MS 60-3
   NASA Lewis Research Center
   21000 Brookpark Road
   Cleveland, Ohio 44135

2. Technology Utilization
   MS 3-19
   NASA Lewis Research Center
   21000 Brookpark Road
   Cleveland, Ohio 44135

3. NASA Rep. RQT-2448 (6)
   NASA Scientific-Technical Information Facility
   P. O. Box 3300
   College Park, Md. 20740

4. Library
   NASA Flight Research Center
   P. O. Box 273
   Edwards, California 93523

5. Library
   NASA
   Manned Space Flight Center
   Houston, Texas 77058

6. Patent Counsel
   MS 500-311
   NASA Lewis Research Center
   21000 Brookpark Road
   Cleveland, Ohio 44135

7. Mr. G. C. Deutsch/RRM
   NASA Headquarters
   600 Independence Avenue
   Washington, D.C. 20546

8. Library
   NASA
   Ames Research Center
   Moffett Field, California 94035

9. Library
   Jet Propulsion Laboratory
   4800 Oak Grove Drive
   Pasadena, California 91102

10. Library
NASA
Marshall Space Flight Center
Huntsville, Alabama 35812

11. Report Control Office
MS 5-5
NASA Lewis Research Center
21000 Brookpark Road
Cleveland, Ohio 44135

12. Mr. N. Rekos/RAP
NASA Headquarters
600 Independence Avenue
Washington, D.C. 20546

13. Library
NASA
Goodard Space Flight Center
Greenbelt, Maryland 20771

14. Library
NASA
Langley Research Center
Langley Field, Virginia 23365